# Overview of Experimental Results on the HL-2A Tokamak

L.W. Yan 1), X.R. Duan 1), X.T. Ding 1), J.Q. Dong 1), Q.W. Yang 1), Yi Liu 1), X.L. Zou 2), D.Q. Liu 1), W.M. Xuan 1), L.Y. Chen 1), J. Rao 1), X.M. Song 1), Y. Huang 1), W.C. Mao 1), Q.M. Wang 1), Q. Li 1), Z. Cao 1), B. Li 1), J.Y. Cao 1), G.J. Lei 1), J.H. Zhang 1), X.D. Li 1), W. Chen 1), J. Cheng 1), C.H. Cui, 1) Z.Y. Cui 1), Z.C. Deng 1), Y.B. Dong 1), B.B. Feng 1), Q.D. Gao 1), X.Y. Han 1), W.Y. Hong 1), M. Huang 1), X.Q. Ji 1), Z.H. Kang 1), D.F. Kong 3), T. Lan 3), G.S. Li 1), H.J. Li 1), Qing Li 1), W. Li 1), Y.G. Li 1), A.D. Liu 3), Z.T. Liu 1), C.W. Luo 1), X.H. Mao 1), Y.D. Pan 1), J.F. Peng 1), Z.B. Shi 1), S.D. Song 2), X.Y. Song 1), H.J. Sun 1), A.K. Wang 1), M.X. Wang 1), Y.Q. Wang 1), W.W. Xiao 1), Y.F. Xie 1), L.H. Yao 1), L.Y. Yao 1), D.L. Yu 1), B.S. Yuan 1), K.J. Zhao 1), G.W. Zhong 1), J. Zhou 1), Y. Zhou 1), J.C. Yan 1), C.X. Yu 3), C.H. Pan 1), Yong Liu 1) and HL-2A team

1) Southwestern Institute of Physics, Chengdu, China
2) CEA, IRFM, Cadarache, France
3) University of Science and Technology of China, Hefei, China

E-mail contact of main author: lwyan@swip.ac.cn

Abstract. The physics experiments on the HL-2A tokamak have been focused on confinement improvement, particle and thermal transport, zonal flow and turbulence, filament characteristics, energetic particle induced modes, and plasma fueling efficiency since 2008. ELMy H-mode discharges are achieved using combination of NBI heating with ECRH. The power threshold is found to increase with decrease of density, almost independent of the launching order of the ECRH and NBI heating power. The pedestal density profiles in the H-mode discharges are measured. The particle outward convection is observed during pump-out transient phase with ECRH. The negative density perturbation (pump-out) is observed to propagate much faster than the positive one caused by out-gassing. The core electron thermal transport reduction triggered by far-axis ECRH switch-off is investigated. The coexistence of low frequency zonal flow (LFZF) and geodesic acoustic mode (GAM) is observed. The dependence of the intensities of LFZFs and GAMs on safety factor and ECRH power is identified. The 3D spatial features of plasma filaments are measured and large-scale structures along a magnetic field line analyzed for the first time. The beta-induced Alfvén eigenmodes (BAEs), excited by large magnetic islands (m-BAE) and by energetic electrons (e-BAE), are observed. The frequency of the beta-induced Alfvén acoustic eigenmode (BAAE) identified in experiment is in agreement with theoretical prediction. The results for the study of fueling efficiency and penetration characteristics of supersonic molecular beam injection (SMBI) are described.

Key words: ELMy H-mode, cross field transport, zonal flow, energetic particles, SMBI

## 1. Introduction

Magnetically confined fusion research activities may be divided into two general aspects. One is to confirm the ITER physics and technology basis by combining the known elements of tokamak plasma physics into so-called integrated operation scenarios [1]. The other is to

prepare for a fruitful ITER scientific programme and in view of an optimization of the tokamak concept for longer term developments towards DEMO stage and commercial reactors. The former aspect is coincident with the scientific missions of HL-2A [2] experiments for addressing key physics issues relevant to ITER [3]. Several extensive and advanced diagnostic systems such as Thomson scattering and microwave reflectometry have been installed gradually in recent years. A variety of fuelling techniques (extruded pellet injector with 40 pellets, SMBI, gas puffing) and heating systems, such as NBI (1.5 MW/45 keV) and ECRH (3 MW/68 GHz), are developed or improved. The highest discharge parameters achieved are toroidal magnetic field $B_t$ = 2.7 T, plasma current $I_p$ = 430 kA, discharge duration $\tau_d = 4.3$ s, line-averaged density $\bar{n}_e = 6 \times 10^{19}$ m$^{-3}$, electron and ion temperatures $T_e$=5 keV and $T_i$=2.8 keV, respectively. The recent experiments are focused on exploration of L-H transition mechanisms, perturbative study of particle and thermal transport, zonal flow formation and interaction with ambient turbulence, filament characteristics, energetic particle induced modes, and plasma fueling efficiency. The main experimental results obtained since the last IAEA FEC are overlooked in this work while the details are described in corresponding 8 presentations.

The remainder of this paper is arranged as follows. The results of the H-mode experiments are presented in section 2. The observations for particle transport study with modulated ECRH and core heat transport reduction triggered by ECRH switch-off are given in section 3. The newest results on zonal flow and filament characteristics are demonstrated in section 4. The energetic particle driven modes, including the beta-induced Alfvén eigenmodes (BAEs) excited by energetic electrons and by large magnetic islands, and the beta-induced Alfvén acoustic eigenmode (BAAE), are discussed in section 5. The results for plasma fueling efficiency are described in section 6 while section 7 is devoted to a conclusive summary.

## 2. Characteristics of H-mode discharges

The first H-mode discharge was observed on ASDEX in 1982 [4]. The energy confinement time in the discharge was shown to increase to twice of that in L-mode discharges and close to that in Ohmic discharges. Later, H-mode discharges were realized in other tokamaks and some stellarators, using NBI, ICRH, ECRH, even if only Ohmic heating [5]. There is a power threshold for triggering an L-H transition, which depends on magnetic field configuration, bulk ion species, wall condition, fueling location, direction of the magnetic gradient drift of the ions, etc [6]. Recent experiments on ASDEX Upgrade clearly indicate that the power threshold rises with the drop of plasma density [7]. Therefore, quite a few fundamental physics issues of the L-H transition remain open. It is important and urgent to improve our understanding for L-H transition power threshold and the issues such as transition triggering mechanism, driving forces and control schemes for the ELMs, pedestal structure, etc.

The ELMy H-mode discharges were achieved on HL-2A using the NBI heating and ECRH of the 2$^{nd}$ harmonic X-mode in 2009 after other discharge conditions had been optimized [8]. Many methods are tested to reduce the power threshold. The H-mode discharges with the

ELM periods less than 15 ms are reproducible. The pre-transition plasma density is rather crucial, which is limited to (1.2-1.8) $\times 10^{19}$ $m^{-3}$ due to the use of ECRH. The minimum power threshold is about 1.1 MW at the density of 1.6 $\times 10^{19}$ $m^{-3}$, which is about four times of the predicted power threshold.

The SMBI is used to fuel plasma because it has higher fueling efficiency, deeper penetration, and lower recycling than normal gas puffing [9]. An H-mode discharge with 6 SMBI pulses is shown in *FIG. 1*. The first SMBI pulse makes the $D_\alpha$ in divertor decrease slightly even if the density increases. The ECRH power of 450 kW added at t = 425 ms leads to central electron density drop and radiation power rise clearly. The neutral beam of 460 kW is injected into plasma at t = 510 ms. Immediately, the stored energy and radiation power start to rise followed by plasma density rise at t = 530 ms after the second SMBI pulse, and then the discharge enters an H-mode phase from t = 550 ms. The available data indicate that power threshold is reduced at least 10% by the SMBI fueling in comparison with the gas puffing. One of the possible mechanisms is that the SMBI can induce higher particle flux across the LCFS and thus reduce required energy flux for the transition as predicted by the theories [10, 11].

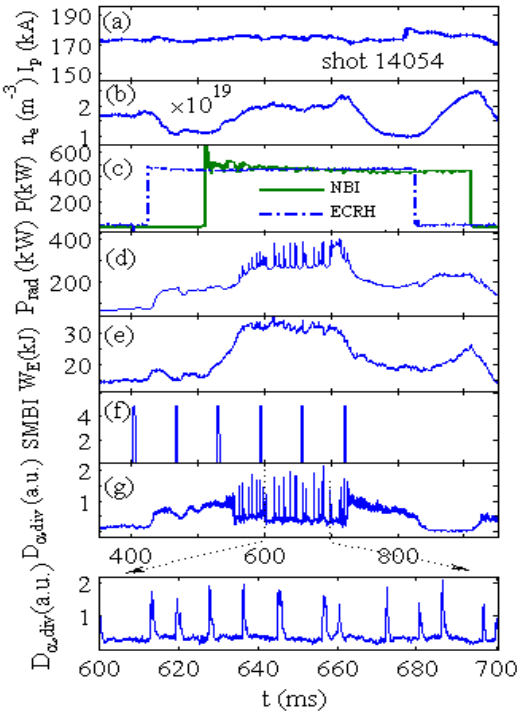


*FIG. 1. The H-mode with the SMBI fueling in discharge 14054. The waveforms from top to bottom are, the plasma current (a), central line-averaged electron density (b), NBI and ECRH powers (c), radiation power in main chamber (d), stored energy (e), SMBI pulses (f), $D_\alpha$ emissions in divertor (g) and a zoomed part of it, respectively.*

The typical ELM periods are 1-3 ms with exceptions of more than 10 ms [12]. The parameter evolutions with ELMs in discharge No.14054 are illustrated in *FIG. 2*. The curves from the top to the bottom are the line-averaged density, the poloidal beta, the stored energy, confinement time and $D_\alpha$ emission in the divertor. The maximum ELM period is 12 ms, the corresponding poloidal beta, stored energy and energy confinement time all decrease 10 % although the density reduces only ~ 5 %. The energy confinement time limited by the ELMs is estimated as 120 ms, which is much longer than the confinement time (~28 ms) from diamagnetic measurement.

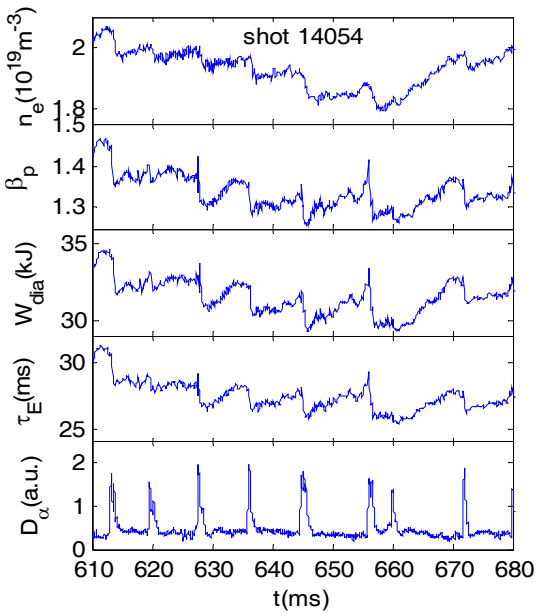


*FIG. 2. Main parameter evolutions during ELM phase in discharge 14054.*

The measurement of pedestal width is quite difficult because it needs rather high spatial resolution of diagnostics. Fortunately, the density pedestal width of ~ 2.8 cm is measured by using microwave reflectometry of O-mode and a Langmuir probe array in discharge 14052, as shown in *FIG. 3*. The pedestal density is $1.25\times10^{19}$ $m^{-3}$, which is 60 % of line-averaged density ($2\times10^{19}$ $m^{-3}$). The power threshold of the L-H transition tends to increase with the decrease of plasma density, which is consistent with the recent results on ASDEX Upgrade. The H-mode has been sustained for more than ten times of the energy confinement time, which is mainly limited by auxiliary heating duration. The discharge parameters are extended after entering the H-mode phase.

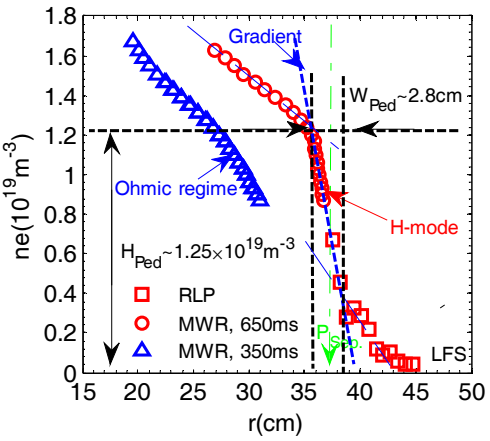


*FIG. 3. Pedestal density width in discharge 14052.*

## 3. Transport study with ECRH

### 3.1 Particle transport investigation with ECRH modulation

Particle transport is one of the key subjects in tokamak physics studies.The particle pump-out phenomenon, characterized by a negative density perturbation in core region, has been observed in ECRH discharges on several tokamaks [13, 14]. As shown in reference [15] density modulation is an effective way to determine the particle diffusivity and convective velocity separately. It is also a useful tool to investigate the particle transport barrier [16]. A few scenarios for the density pump-out induced by ECRH have been carried out in HL-2A [17]. A strong correlation between turbulent increase and density pump-out is noted. Turbulent reduction is observed during the pump-out/pinch transition. The edge density modulation is in phase with ECRH power modulation, while the central one is out of phase.

*Figure 4* shows the amplitude and phase of the first harmonic of the density fluctuation induced by modulated ECRH in limiter (a) and divertor (b) configurations, respectively. The former has a positive density perturbation, which lies at the plasma edge due to out-gassing (a = 37 cm). The simulation [18] shows that the positive perturbation propagates from the edge to the center during the pump-out transient phase, extending over two distinct regions: the peripheral region of inward convection (33 cm < r < 37 cm) with $D_2 = 0.8$ $m^2/s$, $V_2 = 15$ m/s, and the core region of outward convection (28 cm < r < 33 cm) with $D_1 = 0.4$ $m^2/s$, and $V_1 = -4$ m/s. The divertor configuration has negative particle source located at the core region, propagating from the center to the edge with D = 1.5 $m^2/s$, and V = -10 m/s. The observations clearly indicate that the negative density perturbation propagates faster than the positive one. This strong asymmetry between the positive and negative density perturbations resembles that observed in thermal transport studies with hot and cold pulses.

It should be noted that the particle convection is always inward before and after the pump-out phase and that the outward convection is only observed in the pump-out transient phase.

Theoretical research indicates that the turbulence driven by trapped electron mode (TEM) can lead to an outward convection via thermodiffusion [19]. Thus the previous observation can be a crucial indication for the TEM presence during the pump-out. The particle transport during ECRH is also investigated with SMBI modulation.

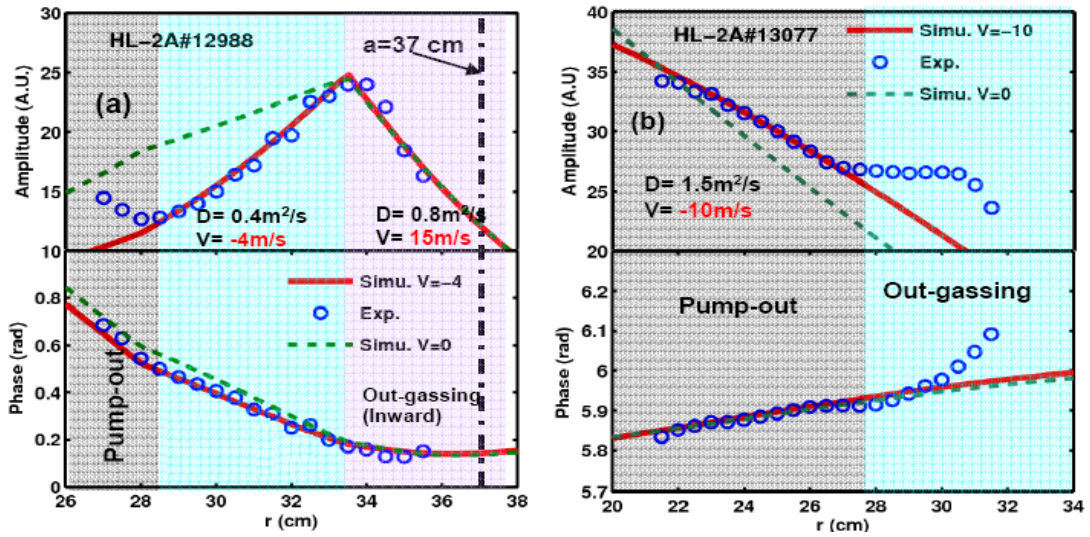


*FIG. 4. The amplitude and phase of the first harmonic of the density modulation wave by ECRH in a limiter configuration (a) and a divertor configuration (b). Open circle is the experimental data; the solid lines represent the simulation with convection; the dash lines are the simulation without convection (V=0) in the corresponding domain.*

### 3.2 Core transport reduction triggered by ECRH power switch-off

The experiments performed on various devices have shown core thermal transport reduction triggered by the localized ECRH [20]. A large increase of central electron temperature is induced by off-axis ECRH in DIII-D [21]. Observations in T-10 and TEXTOR show that the necessary condition for reduction of core transport is related to the appearance of low magnetic shear near rational flux surfaces [22, 23]. However, previous off-axis ECRH experiments in several devices was mostly carried out around r/a~0.4. However, it is still unclear about the link among the improvement confinement, the ECRH power deposition and the core turbulence.

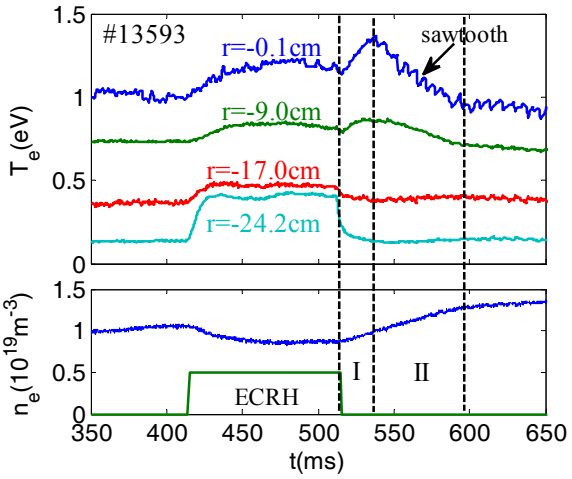


*FIG. 5. Confinement improvement triggered by far off-axis ($r_{dep}/a$ =0.69) ECRH switch-off.*

The experiments with various ECRH depositions by changing the toroidal field have been conducted in HL-2A [24]. The central temperature drop time delay is found to increase with

the radius of the ECRH deposition position. It is also found that the central electron temperature suddenly increases and then remains for several tens of milliseconds before it starts to decrease after the far off-axis ECRH switch-off (see *FIG. 5*). A thermal barrier is observed near the q= 1 rational surface. The corresponding transport is decreased by a factor of two. This is related to the significant suppression of core turbulence, as shown in *FIG. 6*. The turbulence power spectrum near the q = 1 surface after ECRH switch-off is much lower than that before or during ECRH, implying that the central turbulence is suppressed after far-axis ECRH switch-off.

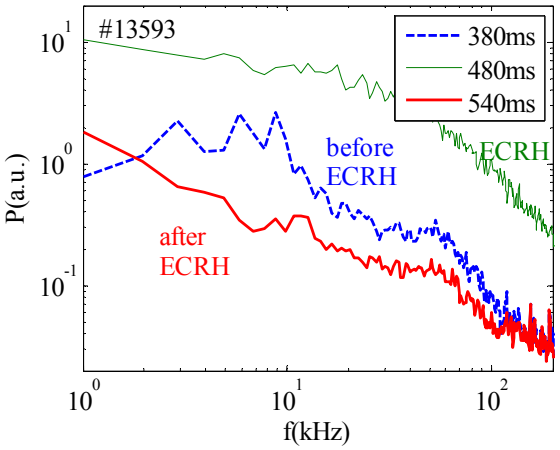


*FIG. 6. Turbulence power spectra near q = 1 surface before, during, and after ECRH. The ECRH power deposited at $r_{dep}/a$ ~0.69.*

## 4. Zonal flows and filament characteristics

### 4.1 Low frequency zonal flows and geodesic acoustic mode

Zonal flows became one of the key topics in magnetic fusion plasma sciences in the last decade in theory [25] and experiment [26]. The spectral characteristics of low frequency zonal flows (LFZFs) [27] and geodesic acoustic modes (GAMs) [28-31] were studied using Langmiur probe arrays in HL-2A Ohmic and ECRH plasmas. Given in *FIGs. 7(a)* and *(b)* are the auto-power spectra of the floating potentials, which are roughly proportional to radial electric field power spectra [32]. The LFZF intensities increase but the GAMs decrease when the edge safety factor q decreases from 6.2 to 3.5. On the other hand, the intensities of the LFZFs and GAMs increase while the ECRH power increases from 380 to 680 kW when the q is fixed. The radial profile of the LFZF intensity in ECRH plasma is studied and compared with that in Ohmic plasma. Shown in *FIG. 8(a)* are the radial profiles of the LFZF radial electric field power density in Ohmic (squares) and ECRH (circles) plasmas. The same

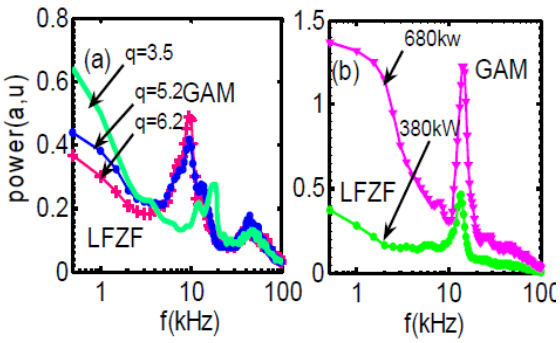


*FIG. 7. The Auto-power spectra of floating potentials versus (a) safety factor q, and (b) ECRH power.*

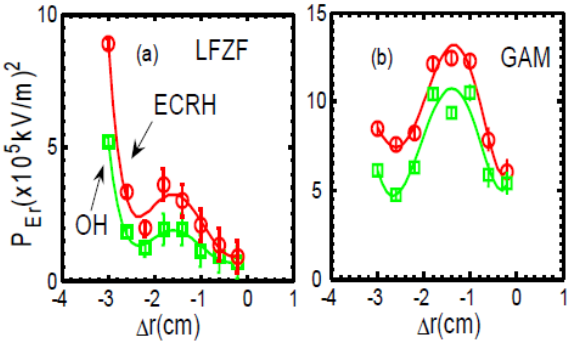


*FIG. 8. The power density of radial electric field fluctuations versus radial position for the LFZF (a) and GAM (b) in OH and ECRH (of power 150 kW) plasmas.*

profiles for the GAM are given in *FIG. 8(b)*. Moving from the boundary inwards, the intensity of LFZF first increases slightly and then sharply rises at the location of ~2.5 cm inward from the last closed flux surface (LCFS) where the GAM power reaches a minimum. On the other hand, the power of GAMs has a maximum at ~1.5 cm inward from the LCFS. The spatial properties of the turbulent envelopes, including long range correlation, poloidal and toroidal symmetries and finite radial wave number, are similar to those of zonal flows themselves. An anti-phase correlation is clearly revealed between the waveforms of LFZF and turbulence envelope in LFZF frequency region in ECRH plasma.

### 4.2. Filament characteristics

Plasma filaments or blobs are one of the main sources for cross-field transport in boundary plasmas of fusion devices [33]. The inward convection due to density hole has been observed in JET [34]. The filament experiments on HL-2A were performed in ohmically heated deuterium discharges with five probe array [35]. Interchange modes and strong sheared flows are considered as the plausible mechanism for the filament formation. Recently, a novel probe combination of poloidal 10-tip array (Array A) with radial 8-tip array (Array B), separated by 210 cm toroidally, is used to measure the 3D spatial structures of the filaments [36]. A magnetic field line passing a tip in the Array A can intersect another tip in the Array B for a suitable magnetic field $B_t$ and plasma current $I_p$. *Figure 9(a)* shows the contour plot of the cross correlation between arrays, where $\Delta d_\theta$ is the poloidal distance between tip 1 and another tip in Array A. The peak of maximum cross-correlation appears at tip 5 with poloidal separation of $\Delta d_\theta$ ~16 mm from tip 1 and at the radial position of $\Delta r$ = 16 mm outward from the LCFS. *Figures 9(b)* and *9(c)* give the maximum coherency and the averaged parallel wave number ($k_{//}$) between each tip in Array A and the tip fixed at $\Delta r$ = 16 mm in Array B. The maximum poloidal coherency reaches 0.91 at the position of $d_\theta$ = 16 mm, indicated by the vertical dash line, is close to an ideal field line. The wave number changes sign at the $d_\theta$ = *16* mm, indicating the existence of zero parallel wave number ($k_{//}$ = 0) relevant to interchange mode.

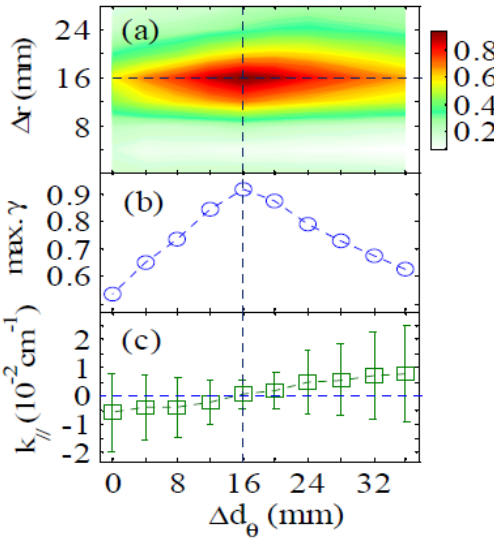


*FIG. 9. The contour of maximum cross-correlation between arrays (a), the maximum coherency (b) and averaged parallel wave number (c) between tips.*

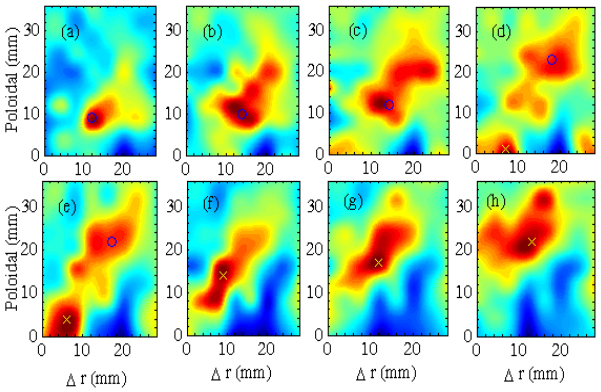


*FIG. 10. The 2D images for conditional average of floating potentials measured with poloidal 10-tip and radial 8-tip arrays at 8 different delay times. The adjacent time interval is 5 μs.*

The above two probe arrays are used to study filament propagation based on significant parallel coherency. *Figure 10* show 2D plasma images in poloidal-radial plane outside magnetic separatrix. The first filament (marked by a circle) appears into the observation region with poloidal and radial sizes less than 10 mm, as shown in *FIG. 10(a)*, and then its amplitude gradually grows, as seen in *FIG. 10(b)* and *FIG. 10(c)*. Meantime, the second filament appears (denoted by a cross) in *FIG. 10(d)*, which has a separation of 25 mm from the first one. *Figure 10(e)* illustrates that the second filament gradually moves into the observation zone, and the distance between them becomes smaller, implying that the second filament goes faster than the first. It should be noted that the first filament almost disappears in *FIG.10(f)*, suggesting the filament lifetime to be about 25 μs. *Figure 10(g)* and *10(h)* display the continuous movement of the second filament. Another obvious feature is the inclination of 2D structure.

## 5. Energetic particle induced modes

### 5.1 Beta-induced Alfvénic eigenmode

The Alfvénic instabilities can be driven by energetic particles in future fusion reactors, such as ITER and DEMO. The instabilities may lead to significant loss of energetic particles and harm the first wall, and therefore, are very important subject in current tokamak physics. Most probable theoretic identifications of the BAE excited by beam ions have been proposed: a discrete shear Alfvén eigenmode (AE), a kinetic ballooning mode (KBM) and a hybrid mode between Alfvénic and KBM branches or between Alfvénic and ion acoustics branches [37]. The BAEs were first observed in DIII-D [38] and then in TFTR plasmas with fast ions [39]. Subsequently, the BAEs were reported in FTU with strong tearing mode activity [40] and in TEXTOR Ohmic plasmas without fast ions [41]. Recently, the BAEs were observed during a sawtooth cycle in ASDEX-U [42] and TORE-SUPRA plasmas with fast ions [43].

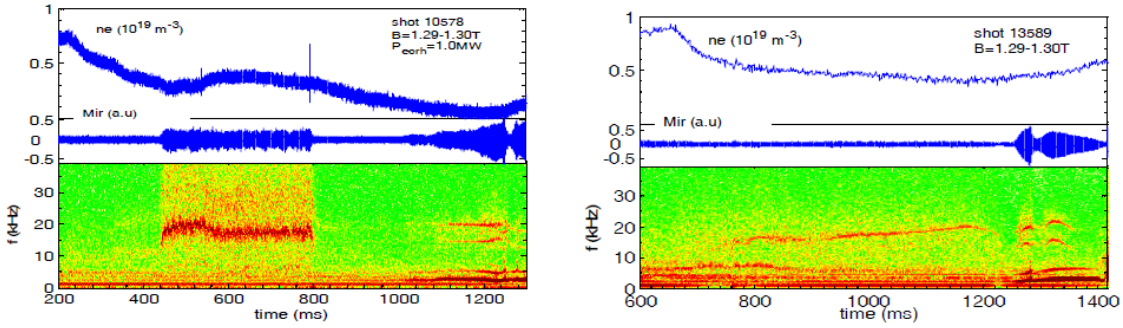


*FIG. 11. The BAEs excited by energetic electrons in 440-790 ms with ECRH and by large magnetic island in 1090-1250 ms without ECRH (left); The BAEs in Ohmic plasma without large island in 730-1225 ms and excited by large magnetic island in 1260-1360 ms (right).*

*Figure 11* shows the BAEs excited by large magnetic islands (m-BAEs) and energetic electrons (e-BAEs) in HL-2A [44, 45]. The m-BAEs with mode numbers of m/n = 2/1 and -2/-1 propagate poloidally and toroidally in opposite directions, and form standing-wave structures in the island frame. There is a threshold of magnetic island width for the m-BAEs, whose frequencies are proportional to the island width. The e-BAE has mode number of m/n

= -3/-1, propagating poloidally in the electron diamagnetic drift direction and toroidally opposite to the plasma current in the laboratory frame. The mode frequency is close to the frequency of the m-BAEs. The e-BAE excitation is related not only with the population of the energetic electrons, but also to their energy and pitch angles. To identify the frequencies of the BAEs, the generalized fishbone-like dispersion relation (GFLDR) [46] and magnetic-island-induced dispersion relation [47] have been solved near marginal stability, respectively. The observed frequencies are in agreement with theoretical results.

The BAE frequency can be estimated at the continuum accumulation point (CAP) of the low frequency gap induced by the shear Alfvén continuous spectrum due to finite beta effect, which provides an upper bound for the expected mode frequencies. The frequency $f_{CAP}$ versus ion temperature at the $q = 3$ surface is shown in *FIG. 12*. The e-BAE frequency at the accumulation point is $f_{CAP} \approx 19$ *kHz* ($\tau \equiv T_e / T_i = 1$) or $f_{CAP} \approx 22$ *kHz* ($\tau = 2$), while the observed frequency of the m/n = -3/-1 mode is about $f$ = 18 *kHz* with $T_i$ = 0.15 keV. It is obvious that the observed frequency coincides with the theoretical prediction based on the solution of GFLDR. This analyzed result supports that the mode is the e-BAE instability.

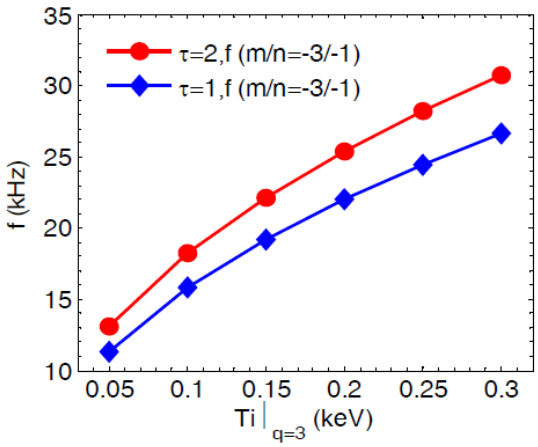


*FIG. 12. The e-BAE frequency at accumulation point versus ion temperature at q=3 surface.*
( ● $\tau \equiv T_e / T_i = 2$; ◆: $\tau \equiv 1$ ).

### *5.2.* Beta-induced Alfvén acoustic eigenmode

The researches indicate that slowly rotating MHD modes can degrade confinement of fast ions [48], especially the modes of Alfvénic type in the lowest part of the spectrum in NBI experiments [49]. In HL-2A, significant depletion of total neutron yield is observed in NBI

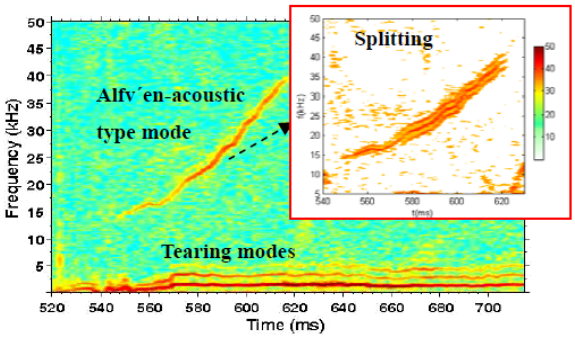


*FIG. 13. Spectrogram of central SXR, showing the low and high frequency modes.*
*The frequency splitting is inserted.*

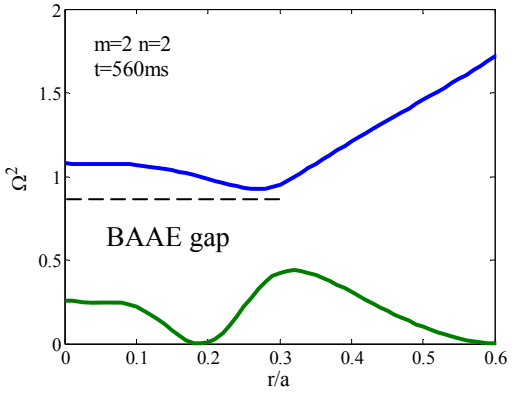


*FIG. 14. Alfvén-acoustic continuum and radial range of the BAAE in HL-2A.*

plasma when the tearing mode instabilities present [50]. A dedicated analysis has revealed the existence of a core localized BAAE with f = 15~40 kHz besides the $m/n$ = 2/1 tearing mode instability, as shown in *FIG. 13*, identified by its frequency up-chirping due to core safety

factor dropping, which is in agreement with numerical solution for Alfvén-acoustic continuum (see *FIG. 14*). Such concurrent multiple modes lead to fast-ion loss. In addition, a clear frequency splitting is first observed for the BAAE (see *FIG.13*), which is strongly relevant to the effect of the resonant wave particle interaction and providing further insight about how frequency splitting structure is generated in plasmas.

## 6. Plasma fueling efficiency

The SMBI fuelling is first developed on HL-1M [51] and then widely adopted by other devices such as Tore Supra [52] and ASDEX-U [53]. On HL-2A, the SMBI can fuel plasma from both low and high field sides (LFS/HFS). The SMBI characteristics from the LFS were measured by a three-lens $D_\alpha$ array and a CCD camera [54]. Its fuelling efficiency is estimated as 40~60% for a limiter configuration and 30-40 % for a divertor configuration. The post-SMBI $D_\alpha$ emission, monitoring the recycling, decreases to 50%, and the neutral pressure in the main chamber drops as well. However, to obtain the same density increment by the gas puffing, the background neutral pressure and edge $D_\alpha$ emission always rise.

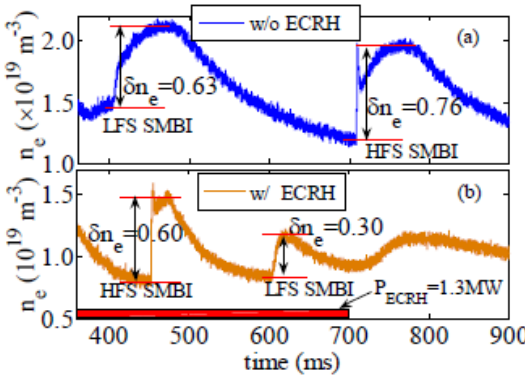


*FIG. 15. Comparison of SMBI fuelling efficiencies between LFS and HFS. (a) and (b) are discharges without and with ECRH, respectively. About $3\times10^{19}$ $D_2$ are injected from both LFS and HFS.*

The comparison of the fuelling efficiencies from LFS and HFS is carried out by injecting identical number of particles [55]. The efficiency from HFS is higher than that from LFS, as shown in *FIG. 15(a)*. Furthermore, when the plasma is heated with the ECRH power of 1.3 MW, the fuelling efficiency drops to about a half for the LFS while it decreases slightly for HFS, as shown in *FIG. 15(b)*. The higher efficiency from HFS may be attributed to magnetic field gradient and curvature drift effects. The perturbation to plasma from HFS is stronger than that from LFS. Among the GP, LFS and HFS SMBIs, it is evident that the HFS SMBI has the highest fuelling efficiency, especially for the plasma heated by powerful ECRH; while the LFS SMBI features relatively high fuelling efficiency and low perturbation to the plasmas.

## 7. Summary

The ELMy H-mode discharges have been achieved on HL-2A with combination of ECRH and NBI heating. The minimum power threshold is about 1.1 MW at the density of $1.6\times10^{19}$ $m^{-3}$. The energy loss can reach 10 % of the total stored energy during an ELM. The typical pedestal width is about 2.8 cm. The SMBI fuelling is found beneficial for triggering L-H transition due to less recycling and deeper penetration than normal gas puffing. The ELMy H-mode has been sustained for more than ten times of the energy confinement time, mainly limited by auxiliary heating duration.

In ECRH discharges, a negative density perturbation due to pump-out process propagates outwards in divertor configuration, while a positive one caused by out-gassing appears in the edge region and propagates inward in limiter configuration. Simulations show possible presence of transiently outward particle convection during pump-out transient phase, and that the negative density perturbation moves faster than the positive one. This strong asymmetry of the negative and positive density perturbations is very similar to that observed in thermal transport studies with hot and cold pulses. In the far off-axis ECRH experiments, immediately after ECRH switch-off, the electron temperature inside the $q$ = 1 surface dramatically increases for several tens of milliseconds before it starts to drop, while the edge temperature drops rapidly. This is related to the significant suppression of core turbulence.

The intensity of the LFZFs is observed to increase and decrease with increases of ECRH power and safety factor q, respectively, while the GAM intensity increases with ECRH power and q. An out-of-phase correlation is clearly revealed between the waveforms of LFZF and turbulence envelope in LFZF frequency region in ECRH plasmas. The 3D spatial structures of plasma filaments are identified with a novel combination of radial and poloidal probe arrays. The significant parallel correlation and near zero parallel wave number are observed, which is in line with the interchange mode driven mechanism. Another feature of plasma filament is inclination propagation in poloidal-radial plane and faster poloidal movement than radial one.

The m-BAEs have been observed to propagate in opposite directions poloidally and toroidally, and form standing-wave structures in an island frame. The e-BAEs driven by energetic electrons are identified for the first time. Both m-BAE and e-BAE routinely appear in the same discharges with close frequencies. A clear frequency splitting is first observed for the BAAE during NBI discharge, whose frequency is in agreement with the numerical solution for Alfvén-acoustic continuum.

The fuelling efficiency of SMBI is estimated as 40~60% for a limiter configuration and 30~40 % for a divertor configuration. The efficiency fuelled from HFS is higher than that from LFS. The former decreases a little but the latter may reduce about a half for high power ECRH plasmas. The perturbation to plasma from HFS is stronger than that from LFS.

References

[1] Shimada, M., et al., Nucl. Fusion 47 (2007) S1.
[2] Liu, Y., et al., Nucl. Fusion 45 (2005) S239.
[3] Duan, X. R., et al., Nucl. Fusion 49 (2009) 104012.
[4] Wagner, F., et al., Phys. Rev. Lett. 49 (1982)1408.
[5] Wagner, F., Plasma Phys. Control. Fusion 49 (2007) B1-33.
[6] Doyle, E. J.,et al., Nucl. Fusion 47(2007) S18.
[7] Ryter, F. et al., Nucl. Fusion 49 (2009) 062003.
[8] Duan, X. R., et al., Nucl. Fusion 50 (2010) 095011.
[9] Yao, L. H. et al., Nucl. Fusion 47 (2007) 1399.
[10] Gohil, P., et al., Phys. Rev. Lett. 86 (2001) 644.
[11] Malkov M.A. and Diamond P.H. 2008 Phys. Plasmas 15 (2008) 122301.

[12] Huang, Y., et al., 23rd IAEA FEC, Daejeon, Korea, 2010, EXS/P3-02.
[13] Weisen, H., et al., Nucl. Fusion 41 (2001) 1227.
[14] Angioni, C., et al., Nucl. Fusion 44 (2004) 827.
[15] Xiao, W. W., et al., Rev. Sci. Instrum. 81 (2010) 013506.
[16] Xiao, W.W., et al., Phys. Rev. Lett. 104 (2010) 215001.
[17] Zou, X.L., et al., 23rd IAEA FEC, Daejeon, Korea, 2010, EXC/P8-20.
[18] Eury, S. P., et al., Phys. Plasmas 12 (2005) 102511.
[19] Garbet, X., et al., Phys. Rev. Lett. 91 (2003) 035001.
[20] Connor, J. W., et al., Nucl. Fusion 44 (2004) R1.
[21] Callen, J.D. et al., Plasma Phys. Control. Fusion 39 (1997) B173.
[22] Hogeweij, G.M.D., et al., Nucl. Fusion 38 (1998) 1881.
[23] Razumova, K.A., et al., Nucl. Fusion 44 (2004) 1067.
[24] Shi, Z. B., et al., 23rd IAEA FEC, Daejeon, Korea, 2010, EXC/P8-14.
[25] Diamond, P. H., et al., Plasma Phys. Control. Fusion 47 (2005) R35.
[26] Fujisawa, A., et al., Nucl. Fusion 49 (2009) 013001.
[27] Liu, A D. et al., Phys. Rev. Lett. 103 (2009) 095002.
[28] Zhao, K.J., et al., Phys. Rev. Lett. 96 (2006) 255004.
[29] Yan, L.W. et al., Nucl. Fusion 47 (2007) 1673.
[30] Lan, T., et al., Plasma Phys. Control. Fusion 50 (2008) 045002
[31] Cheng, J., et al Nucl. Fusion 49 (2009) 085030.
[32] Zhao, K.J., et al., 23rd IAEA FEC, Daejeon, Korea, 2010, EXC/7-3.
[33] Krasheninnikov, S. I. et al., J. Plasma Physics 74 (2008) 679.
[34] Xu, G.S. et al., Nucl. Fusion 49 (2009) 092002.
[35] Cheng, J., et al., Plasma Phys. Control. Fusion 52 (2010) 055003.
[36] Cheng, J., et al., 23rd IAEA FEC, Daejeon, Korea, 2010, EXD/P3-05.
[37] Gorelenkov N.N. and Heidbrink W.W., Nucl. Fusion 42 (2002) 150.
[38] Heidbrink, W.W., et al., Phys.Rev. Lett. 71 (1993) 895.
[39] Heidbrink, W. W. et al., Phys. Plasmas 6 (1999) 1147.
[40] Buratti P., et al., Nucl. Fusion 45 (2005) 1446.
[41] Zimmermann, O. et al., Proc. 32nd EPS Conf., Tarragona, Spain ( 2005) P4.059.
[42] Lauber, Ph., et al., Plasma Phys. Control. Fusion 51 (2009) 124009.
[43] Nguyen, C., et al., Plasma Phys. Control. Fusion 51 (2009) 095002.
[44] Chen, W., et al. Phys. Rev. Lett. 105 (2010), to be published.
[45] Chen, W., et al., 23rd IAEA FEC, Daejeon, Korea, 2010, EXW/4-4Rb.
[46] Zonca, F., et al., Nucl. Fusion 49 (2009) 085009.
[47] Annibaldi, S.V., et al., Plasma Phys. Control. Fusion 49 (2007) 475.
[48] Carolipio, E.M., et al., Nuclear Fusion 42 (2002) 853.
[49] Gorelenkov, N.N., et al., Physics of Plasma 16 (2009) 056107.
[50] Liu, Yi, et al., 23rd IAEA FEC, Daejeon, Korea, 2010, EXW/P7-15.
[51] Yao, L., et al., Nucl. Fusion 38 (1998) 631.
[52] Pégourié, B. et al., J. Nucl. Mater. 313-316 (2003) 539.
[53] Lang, P. T. et al., Plasma Phys. Control. Fusion 47 (2005) 1495.
[54] Yu, D., et al., Nucl. Fusion 50 (2010) 035009.
[55] Yu, D.L., et al., 23rd IAEA FEC, Daejeon, Korea, 2010, EXC/P8-22.